Electronic Supplementary Material (ESI) for Physical Chemistry Chemical Physics.

Supporting information

Spontaneous proton transfer in a series of amphoteric molecules under hydrostatic pressure

Binhong Yu,[a] Yi Wang,[b] Lingrui Wang,[c] Xiao Tan,[c] Yu-Mo Zhang,[a] Kai Wang,[a,c] Minjie Li,[a]* Bo Zou,[c]* Sean Xiao-An Zhang[a]*

[a.] State Key Laboratory of Supramolecular Structure and Materials, Jilin University, Changchun, Jilin 130012, China.
E-mail: liminjie@jlu.edu.cn, seanzhang@jlu.edu.cn.

[b.] Institute of Chemical Materials, China Academy of Engineering Physics (CAEP), Mianyang 621000, China.

[c.] State Key Laboratory of Superhard Materials, Jilin University, Changchun, Jilin 130012, China.
E-mail: zoubo@jlu.edu.cn

Table of Contents

Experimental details

Materials and instruments

Phenylhydrazine, 3-methylbutan-2-one, salicylaldehyde, iodomethane nitrosalicylaldehyde, 3-nitrosalicylaldehyde and 2,3,3-trimethyl-3H-indole were purchased from commercial sources and used without further purification.

Instruments

^{1}H NMR and ^{13}C NMR spectra were recorded on a Varian Mercury using TMS as a standard at room temperature. LC-HRMS analysis was performed on an Agilent 1290-microTOF-Q II mass spectrometer. UV-Vis absorption spectra were measured using a Shimadzu UV-2550 PC double-beam spectrophotometer. Single-crystal X-ray diffraction data was recorded on a Rigaku RAXIS-PRID diffractometer.

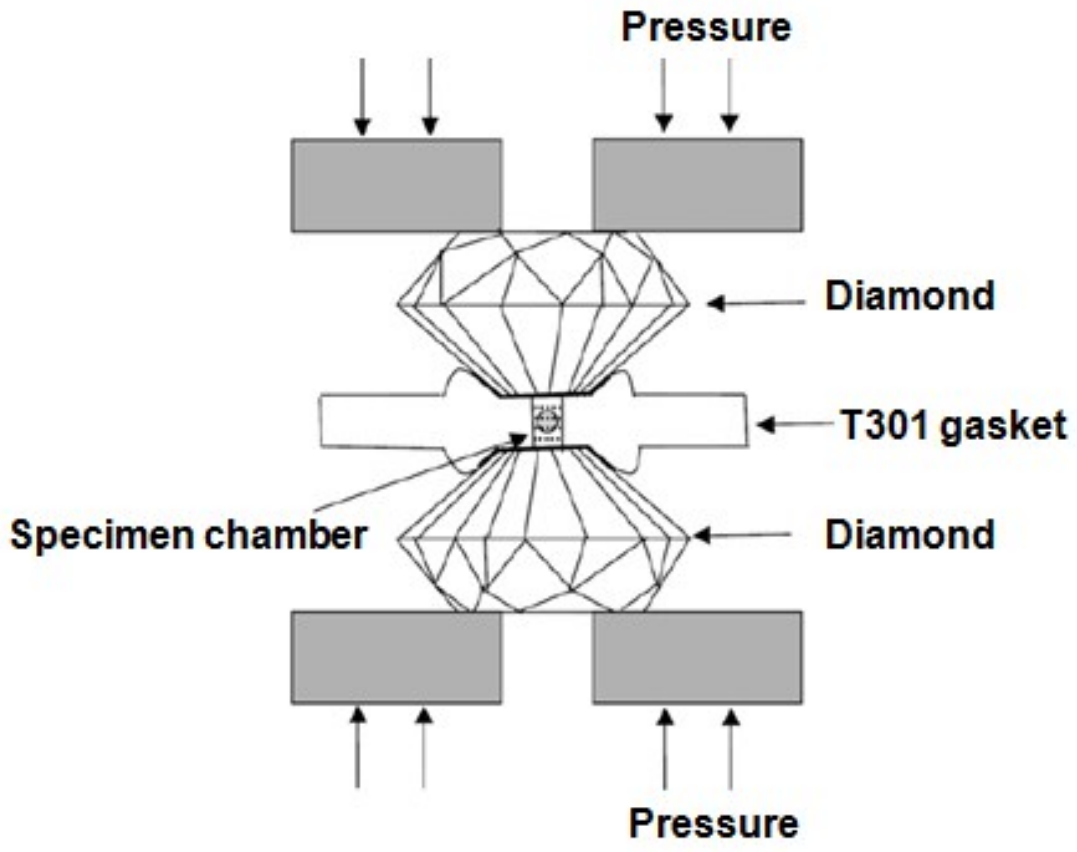

Schematic diagram of diamond anvil cell (DAC)

High-pressure experiments were carried out using a diamond anvil cell (DAC) (detailed descriptions shown as above). The culet diameter of the diamond anvils was 0.5 mm. T301 stainless steel gaskets were preindented to a thickness of 60 μm, and center holes of 0.16 mm were drilled for the sample. The ruby chip was used for pressure determination using the standard ruby fluorescent technique. Silicone oil was used as the pressure-transmitting medium. All experiments were performed at room temperature. High-pressure unpolarized Raman spectra were recorded using Acton SP2500i spectrometer (Princeton Instruments) equipped with the liquid nitrogen cooled CCD (PyLon: 100B). The 532 nm radiation from the diode pumped solid state (DPSS) laser was utilized to excite the sample and the output power was 10 mW. High-pressure absorption spectra were recorded by an optical fiber spectrometer (Ocean Optics, QE65000). The real optical images were obtained by using a Nikon Ti-U microscope equipped with a digital color camera.

Synthesis of AM-N, AM, OM-N, AM-N-C and control molecules

The following products were synthesized according to literature.[1-2]

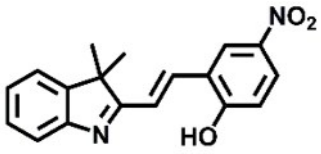

^{1}H NMR (500 MHz, DMSO) δ 11.75 (s, 1H), 8.70 (d, J = 2.5 Hz, 1H), 8.12 (dd, J = 9.0, 2.8 Hz, 1H), 7.99 (d, J = 16.4 Hz, 1H), 7.54 (d, J = 7.6 Hz, 1H), 7.52 – 7.46 (m, 2H), 7.33 (t, J = 7.5 Hz, 1H), 7.23 (t, J = 7.3 Hz, 1H), 7.10 (d, J = 9.0 Hz, 1H), 1.41 (s, 6H). ^{13}C NMR (126 MHz, DMSO-d_6), δ (TMS, ppm):183.73, 162.40, 154.11, 147.17, 140.59, 130.99, 128.11, 126.34, 126.00, 124.08, 123.79, 122.02, 122.02, 120.63, 116.87, 52.85, 23.19, 23.19. LC-HRMS: m/z calcd. $[M + H]^+$ 309.1239, found 309.1240.

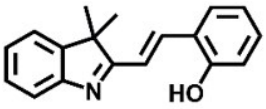

^{1}H NMR (500 MHz, DMSO-d_6) δ 10.08 (s, 1H), 8.01 (d, J = 16.5 Hz, 1H), 7.75 (d, J = 7.4 Hz, 1H), 7.51 (d, J = 7.6 Hz, 1H), 7.46 (d, J = 7.2 Hz, 1H), 7.31 (t, J = 7.3 Hz, 1H), 7.21 (m, 3H), 6.92 (d, J = 8.1 Hz, 1H), 6.87 (t, J = 7.5 Hz, 1H), 1.39 (s, 6H). ^{13}C NMR (126 MHz, DMSO-d_6), δ (TMS, ppm): 184.00, 156.61, 154.30, 147.03, 133.31, 130.98, 128.03, 127.96, 125.60, 123.04, 121.92, 120.31, 119.86, 119.17, 116.52, 52.60, 23.57, 23.57. LC-HRMS: m/z calcd. $[M + H]^+$ 264.1383, found 264.1380.

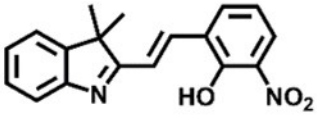

^{1}H NMR (500 MHz, DMSO-d_6) δ 10.94 (s, 1H), 8.27 (d, J = 7.6 Hz, 1H), 8.08 (d, J = 16.4 Hz, 1H), 8.03 (d, J = 8.2 Hz, 1H), 7.57 (d, J = 7.6 Hz, 1H), 7.49 (d, J = 7.2 Hz, 1H), 7.39 (d, J = 16.4 Hz, 1H), 7.34 (t, J = 7.5 Hz, 1H), 7.25 (t, J = 7.3 Hz, 1H), 7.14 (t, J = 8.0 Hz, 1H), 1.41 (s, 6H).^{13}C NMR (126 MHz, DMSO-d_6), δ (TMS, ppm): 183.45, 154.04, 151.13, 147.09, 137.19, 134.12, 130.35, 128.16, 127.89, 126.12, 126.12, 122.16, 122.05, 120.74, 120.34, 52.83, 23.27, 23.27. LC-HRMS: m/z calcd. [M

+ H]$^+$ 309.1234, found 309.1227.

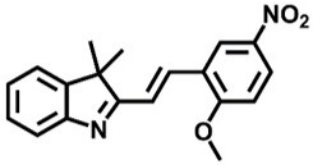

^{1}H NMR (300 MHz, DMSO-d_6): δ (TMS, ppm): 8.75 (d, J = 2.8 Hz, 1H), 8.27 (dd, J = 2.8 Hz, J = 9.2 Hz, 1H), 8.01 (d, J = 16.4 Hz, 1H), 7.57-7.47 (m, 3H), 7.35-7.30 (m, 2H), 7.24 (t, 1H), 4.05 (s, 3H), 1.41 (s, 6H); ^{13}C NMR (126 MHz, DMSO-d_6): δ (TMS, ppm): 183.57, 162.51, 154.07, 147.14, 141.63, 130.08, 128.13, 126.49, 126.11, 125.52, 123.24, 122.80, 122.04, 120.75, 112.70, 57.35, 52.92, 23.04, 23.04. LC-HRMS: m/z calcd. [M+H]$^+$ 323.1390, found 323.1389.

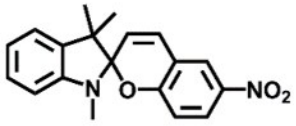

^{1}H NMR (300 MHz, $CDCl_3$) δ (TMS, ppm): 8.04-8.00 (2H, m), 7.21 (1H, t), 7.00 (1H, d, J = 6 Hz), 6.95-6.86 (2H, m), 6.77 (1H, d, J = 10 Hz) 6.56 (1H, d, J = 8 Hz), 5.86 (1H, d, J = 10 Hz,), 2.74 (3H, s), 1.30 (3H, s), 1.19 (3H, s); ^{13}C NMR (125 MHz, $CDCl_3$): δ (TMS, ppm): 159.84, 147.70, 140.94, 136.11, 128.29, 127.87, 125.88, 122.70, 121.66, 121.59, 119.78, 118.68, 115.50, 107.09, 106.39, 52.30, 28.89, 25.91, 19.96. LC-HRMS: m/z calcd. [M + H]$^+$ 323.1390, found 323.1389.

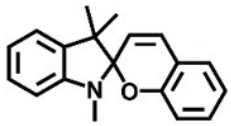

^{1}H NMR (300 MHz, DMSO-d_6): δ (TMS, ppm): 7.17 (1H, dd, J = 7 Hz, 1 Hz), 7.13-7.08 (3H, m), 7.00 (1H, d, J = 10 Hz), 6.85-6.74 (2H, m), 6.66 (1H, d, J = 8 Hz), 6.55 (1H, d, J = 8 Hz), 5.75 (1H, d, J = 10 Hz), 2.65 (3H, s), 1.21 (3H, s), 1.09 (3H, s); ^{13}C NMR (125 MHz, DMSO-d_6): δ (TMS, ppm): 147.67, 147.44, 137.19, 136.28, 132.01, 129.04, 128.01, 125.16, 121.89, 121.74, 121.44, 120.23, 119.89, 107.48, 106.63, 52.21, 28.92, 26.25, 20.08. LC-HRMS: m/z calcd. [M+H]$^+$ 278.1539, found 278.1541.

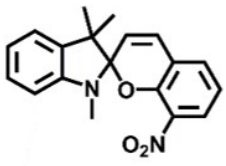

^{1}H NMR (300 MHz, DMSO-d_6): δ (TMS, ppm): 7.70 (1H, d, J = 8 Hz), 7.54 (1H, d, J = 8 Hz), 7.17 (1H, d, J = 10 Hz), 7.13-7.10 (2H, m), 7.03-6.98 (1H, m), 6.80 (1H, t), 6.60 (1H, d, J = 8 Hz), 5.97 (1H, d, J = 10 Hz), 2.67 (3H, s), 1.26 (3H, s), 1.11 (3H, s); ^{13}C NMR (125 MHz, DMSO-d_6): δ (TMS, ppm): 154.42, 148.31, 136.75, 130.23, 129.80, 127.90, 127.39, 121.91, 120.65, 119.68, 119.39, 119.08, 114.80, 107.24, 104.29, 51.81, 29.03, 26.11, 20.34. LC-HRMS: m/z calcd. [M+H]$^+$ 323.1390, found 323.1389.

Table S1. Summary of crystal data and intensity collection parameters for AM-N,[2] AM,[2] OM-N[2] and AM-N-C.

Compound	**AM-N**	**AM**	**OM-N**	**AM-N-C**
Formula	$C_{18}H_{16}N_2O_3$	$C_{18}H_{17}NO$	$C_{18}H_{16}N_2O_3$	$C_{19}H_{18}N_2O_3$
Formula mass	308.33	263.33	308.33	322.35
Space group	P 21/n	P 21/n	P21/c	P ccn
a/ Å	16.289(5)	5.9589(12)	8.578(5)	17.361(4)
b/ Å	5.772(5)	20.362(4)	17.638(5)	25.237(5)
c/ Å	16.527(5)	12.149(2)	10.333(5)	7.5371(15)
α/°	90.000(5)	90	90.000(5)	90
β/°	92.596(5)	92.17(3)	102.223(5)	90
γ/°	90.000(5)	90	90.000(5)	90
V/Å^3	1552.3(15)	1473.0(5)	1527.9(12)	3302.3(11)
Z	4	4	4	8
ρ/g.cm^{-3}	1.319	1.187	1.340	1.297
F_{000}	648	560	648	1360
Temp, (K)	293(2)	293(2)	293(2)	293(2)
Absorption coefficient, μ/mm^{-1}	0.744	0.073	0.093	0.089
No. of reflections measured	8404	10953	6867	28663
No. of independent reflections	2702	2568	3468	3766
R_{int}	0.0617	0.0380	0.0189	0.0692
Final R_1 values ($I > 2\sigma(I)$)	0.0591	0.0640	0.0488	0.0525
Final $wR(F^2)$ values ($I > 2\sigma(I)$)	0.1641	0.1985	0.1188	0.1207
Final $R1$ values (all data)	0.0671	0.0947	0.0698	0.0909
Final $wR(F^2)$ values (all data)	0.1814	0.2310	0.1315	0.1387
Goodness of fit on F^2	1.043	1.101	1.034	1.023
CCDC numbers	**895281**	**895282**	**895283**	**1402973**

Evidence of the proton-transfer process of AM-N, AM and OM-N

Figure S1. The tautomerization between neutral and zwitterionic isomers and absorption spectra of **AM-N, AM, OM-N** and their corresponding control molecules **SP1, SP2, SP3** in solutions with different concentrations or UV irradiation time (365 nm).

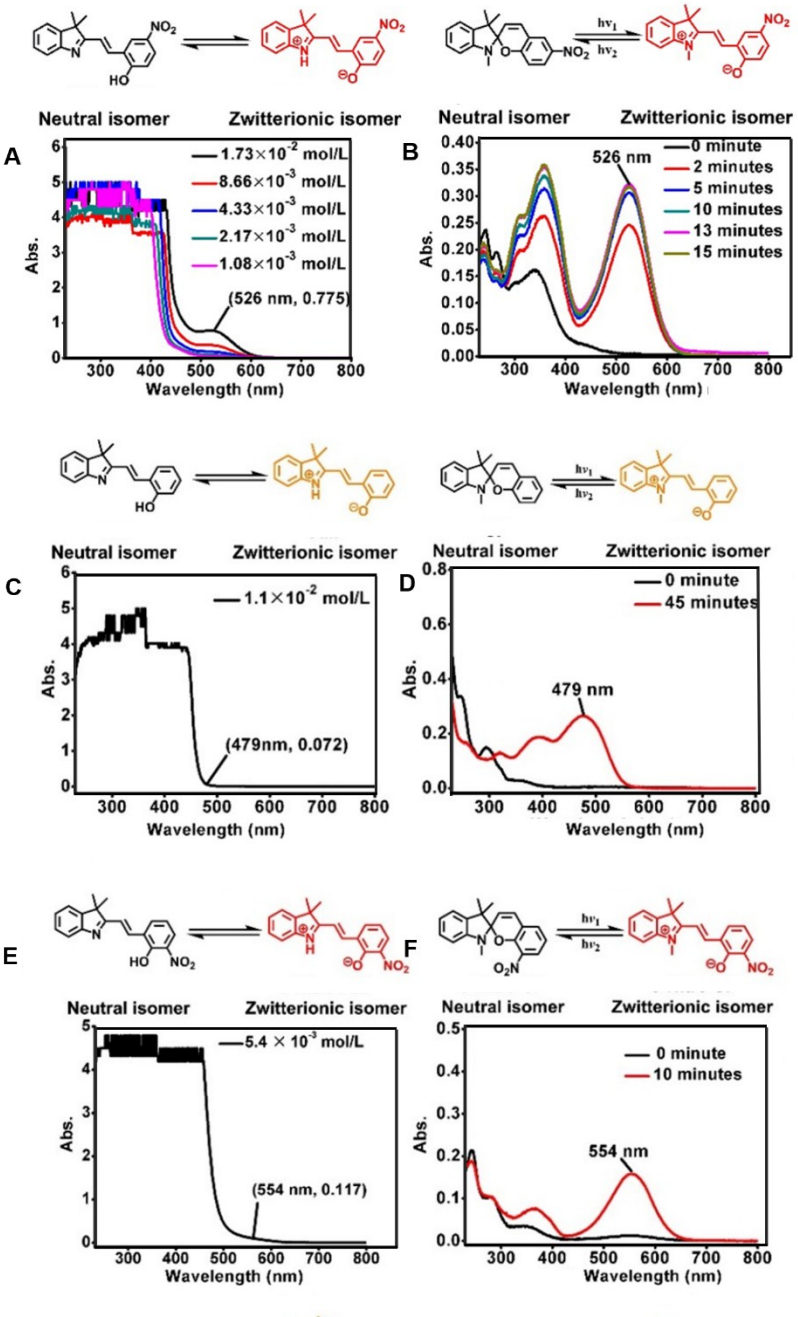

Figure S2. Microscopy images and absorption spectra of **AM-N, AM, OM-N and AM-N-C** before or after grinding.

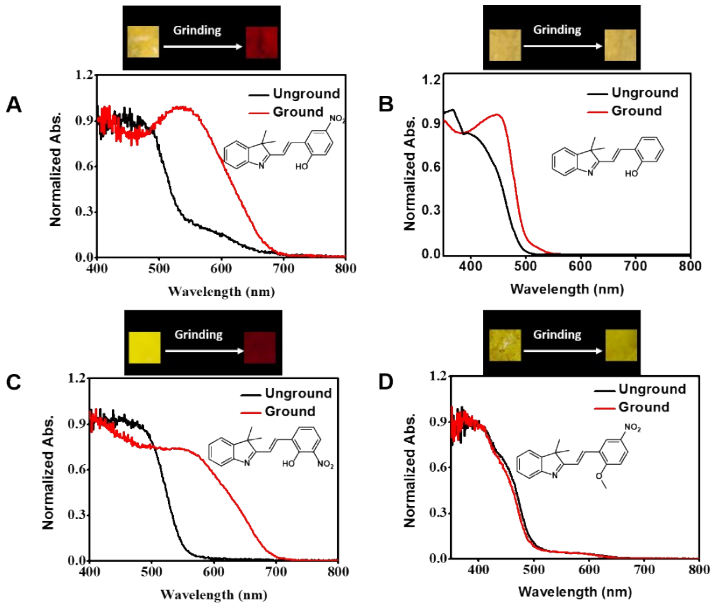

As we know, spiropyrans are well-known photo-responsive molecular switches. Under UV light irradiation, its neutral isomer will transform to the zwitterionic with a new peak in visible light region (Figure S1, right). For example, after UV light irradiation, the new absorption peak (526 nm) of **SP1** appears, which is red-shifted over 100 nm comparable with its neutral from. Interestingly, there are also a shoulder peak around 526 nm in the **AM-N** methanol solutions with high concentrations. Considering the similarity of the conjugated structures in the zwitterionic isomers between **AM-N** and **SP1** (Figure S2a and S2b), the shoulder peak (around 526 nm) in **AM-N** methanol solution should come from small amount of its proton-transferred zwitterionic isomers. The same phenomena that the concentrated **AM** and **OM-N** solution have shoulder peaks near to the corresponding zwitterionic spiropyrans happen, indicating the similar proton-transferred reactions occur. Thus, we consider that there are spontaneous proton-transfer process of **AM-N, AM** and **OM-N** in solution with large scale absorption shifts.

Besides that, in Figure S2, we can observe there are new shoulder peaks of **AM-N** after grinding in the room light. Considering the similarity of the conjugated structures of **AM-N** and **AM-N-C**, we conjure that external force can be able to induce the proton transfer and the neutral-to-zwitterionic transition of **AM-N** in solid state. Based on the similar phenomena of **OM-N** to **AM-N** shown in Figure S2, the proton transfer process of **OM-N** happens, too. However, for the lack of obvious changes after concentrating and grinding, that if there is the proton transfer process of **AM** in solid state can't be determined yet.

Figure S3. The dihedral angles between phenolic plane (yellow) and indole plane (red) for **AM-N** (A), **AM** (B), **OM-N** (C) and **AM-N-C** (D).

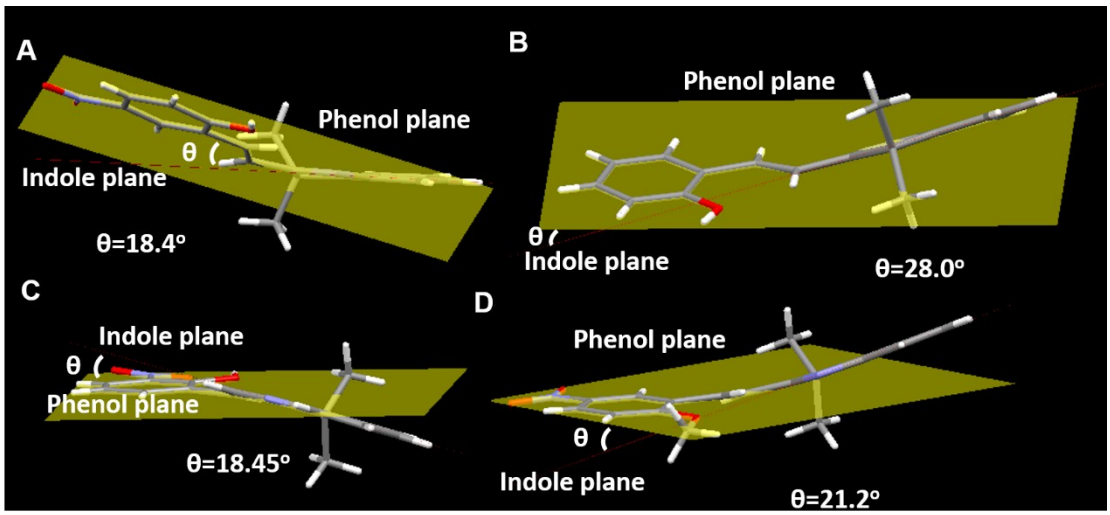

The experimental analysis AM-N under pressure

Figure S4. The difference values between the wavelength at absorption starting-point and main absorption turning-point of AM-N under different pressure. The half point is the point in the absorption spectrum whose intensity is a half of main absorption turning-point's.

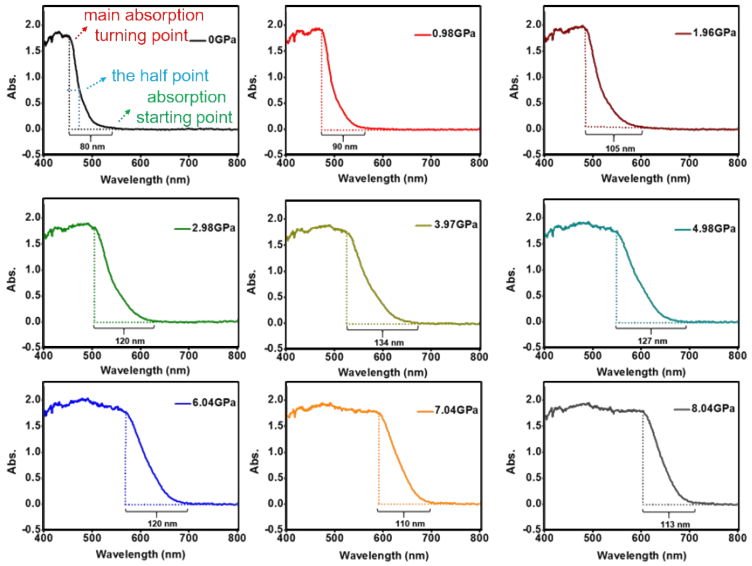

Figure S5. Raman spectra of the **AM-N** crystal in the range of 2700 cm^{-1} to 3700 cm^{-1} under ambient pressure.

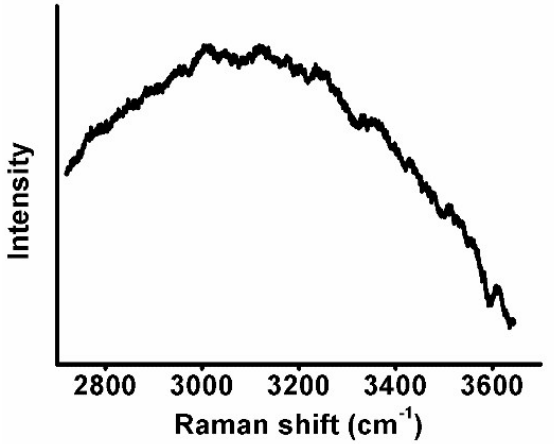

As shown in Figure S5, stretching vibration intensity of phenolic hydroxyl in Raman spectra are so weak that the Raman spectra of the **AM-N** crystal in the range of 2700 cm^{-1} to 3700 cm^{-1} could not be used for structural analysis to make sure the proportion of transformation from neutral isomers to the zwitterionic.

Figure S6. Simulated (A and B) and experimental (C and D) Raman spectra of **AM-N** in neutral form and zwitterionic isomers. The calculations are based on B3LYP/6-31G (d,p), Gaussian 09 package.[3]

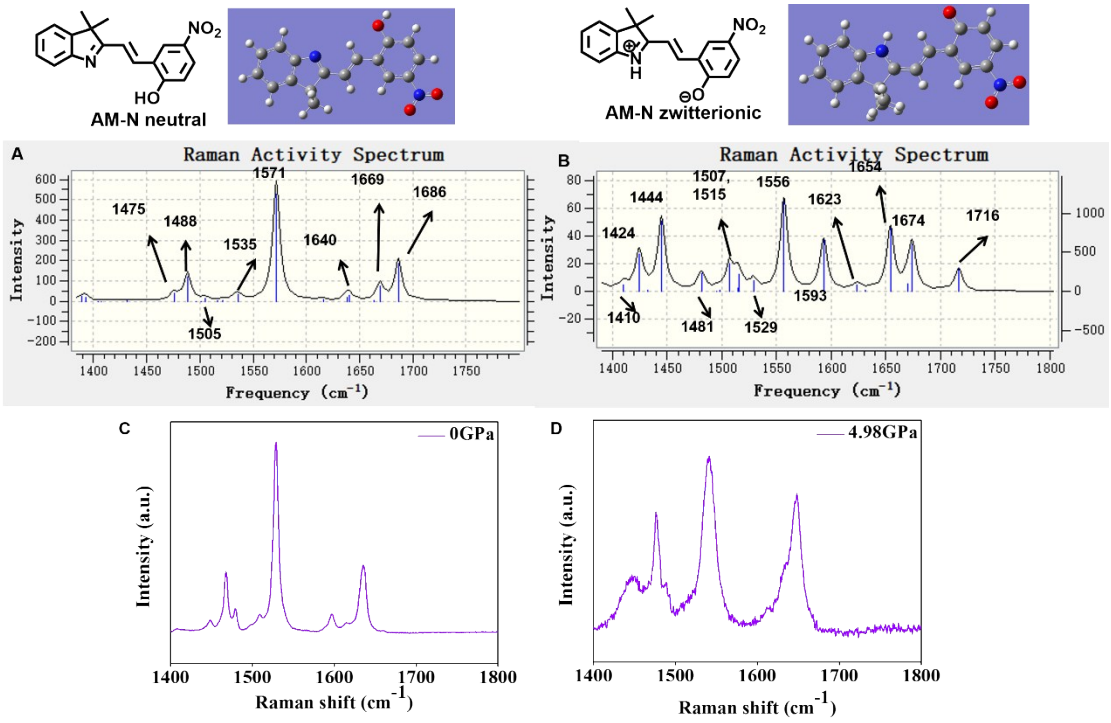

As shown in Figure S6, simulated Raman spectra of neutral AM-N can relatively accurately reflect the experimental results when AM-N is uncompressed. Thus, the

B3LYP/6-31G (d,p) is suitable for our experiments and simulated Raman spectra of zwitterionic AM-N based on this B3LYP/6-31G (d,p) level should be also close to the actual data and we will utilize it to speculate the existing of AM-N under pressure.[3] Through comparing the simulated Raman spectra of AM-N in neutral and zwitterionic isomers, there are some new Raman peaks appear in the Raman spectra of zwitterionic AM-N and these new appeared peaks of zwitterionic AM-N share a common characteristic that their Raman wavenumbers are generally smaller than those of neutral AM-N. Thus, in experimental Raman spectra, the newly appeared Raman peaks with smaller wavenumbers can be assigned to zwitterionic isomers of AM-N (for example, Figure S6D). Moreover, because neutral isomers of AM-N have much stronger Raman activity than those of zwitterionic ones in calculated data, neutral isomers of AM-N will have much stronger Raman peak intensity than that of zwitterionic isomer in experimental Raman spectra, too. To assign the vibration of neutral and zwitterionic AM-N in the range of 1400 cm^{-1} to 1800 cm^{-1}, we have recorded the vibration of main calculated Raman peaks as movie 1, proving the obvious changes upon pressure is resulted from the vibration changes of conjugated π-system from aromatic ring.

Figure S7. (A) Multi-peaks fitting of the Raman peaks of **AM-N** in the range of 1500 cm^{-1} to 1700 cm^{-1}. (B, C) The shifting of the fitted peaks of **AM-N** with pressure. (D) The integrate of fitted Raman spectra of **AM-N**. (E) The ratio of zwitterionic isomer of **AM-N** under high pressure (above 4 GPa).

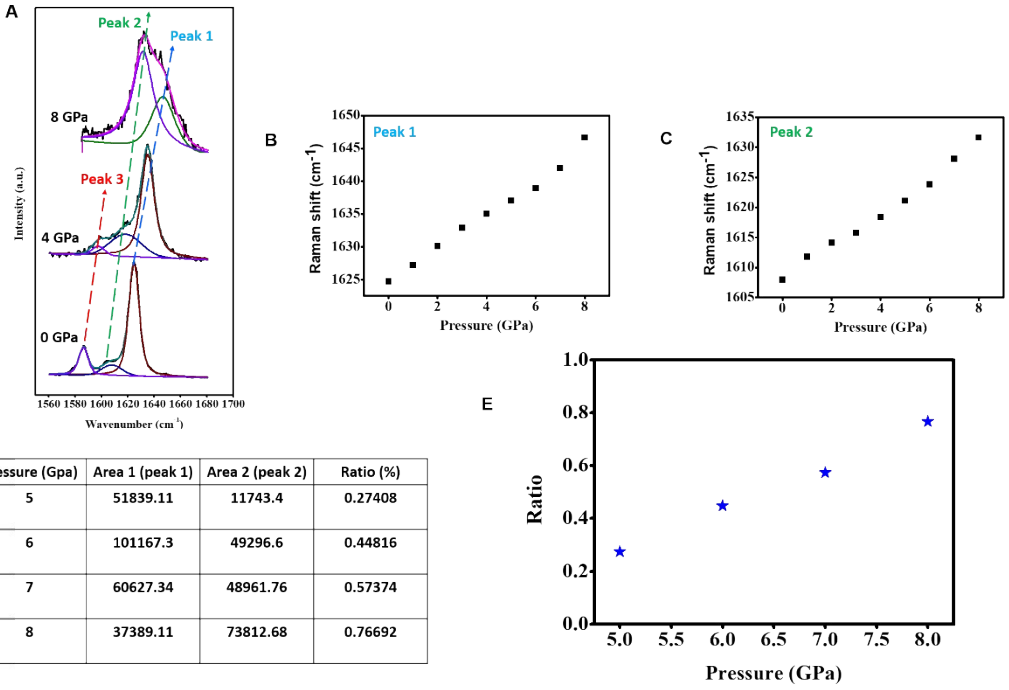

D

Pressure (Gpa)	Area 1 (peak 1)	Area 2 (peak 2)	Ratio (%)
5	51839.11	11743.4	0.27408
6	101167.3	49296.6	0.44816
7	60627.34	48961.76	0.57374
8	37389.11	73812.68	0.76692

Based on the above discussions of Figure S6, Peak 1 and Peak 3 are the characteristic Raman peaks of neutral isomers of **AM-N** while Peak 2 could be assigned to the zwitterionic isomers. Based on the basic principle that the content of one object has a

good linear relation with the intensity of its characteristic Raman peak.[4] During the compression, Peak 2 and Peak 3 are indeed shifting to higher wavenumber with pressure linearly, indicating that neutral isomers of **AM-N** are always existing during whole compression. However, as pressure increases, there is an obvious decreasing integrate of Peak 1 and Peak 3, but increasing integrate of Peak 2. Here, we will utilize the heights of Peak 1 and Peak 2 above 4 GPa to represent the contents of zwitterionic and neutral isomer of **AM-N**, respectively. The ratio of zwitterionic **AM-N** (ω zwitterionic isomer) under high pressure (above 4GPa) could be also roughly estimated by following equation:

$$\omega_{\text{zwitterionic isomer}} = \text{integrate of Peak 2}/(\text{integrate of Peak 2} + \text{integrate of Peak 1}) \times 100\% \ldots 1$$

Equation 1 can be expressed as follow:

$$\omega_{\text{zwitterionic isomer}} = 1/(1 + \text{integrate of Peak 1}/\text{integrate of Peak 2}) \times 100\% \ldots 2$$

Considering the different activity of neutral or zwitterionic isomers of **AM-N**, a correction factor (f) is introduced and the Equation 2 can be expressed as follow:

$$\omega_{\text{zwitterionic isomer}} = 1/(1 + \text{Experimental integrate of Peak 1}/\text{Experimental integrate of Peak 2} \times f) \times 100\% \ldots 3$$

Note: The correction factor (*f*) is obtained through the total Raman activities of simulated Raman peaks for zwitterionic **AM-N** (Figure S6A) divided by the Raman activities of simulated Raman peaks (Figure S6B) for neutral **AM-N**.

$$f = (669+84+825+102+605)/3777 = 0.60$$

Figure S8. In-situ absorption spectra (A) and Raman spectra (B) of the **AM-N** crystal in the DAC with decreasing pressure.

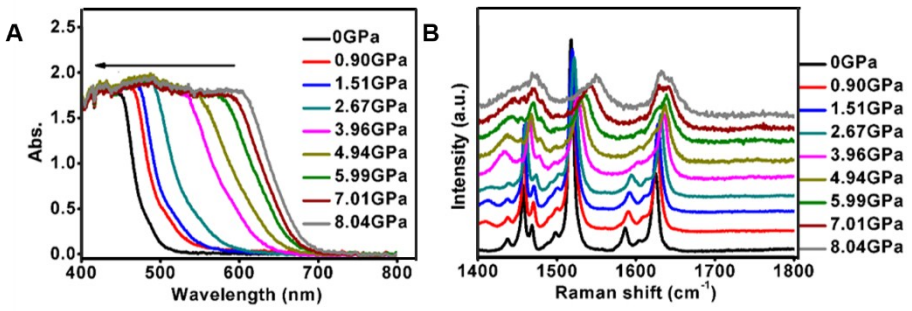

The experimental analysis AM under pressure

Figure S9. The relationship between the wavelength at absorption half-peak height of **AM** crystal and pressure.

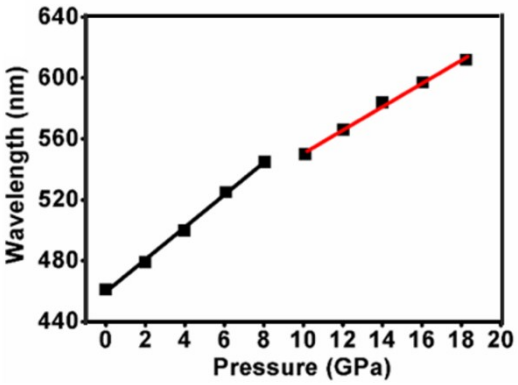

Figure S10. Simulated (A and B) and experimental (C and D) Raman spectra of **AM** in neutral form and zwitterionic isomers. The calculations are based on B3LYP/6-31G (d,p), Gaussian 09 package.[3]

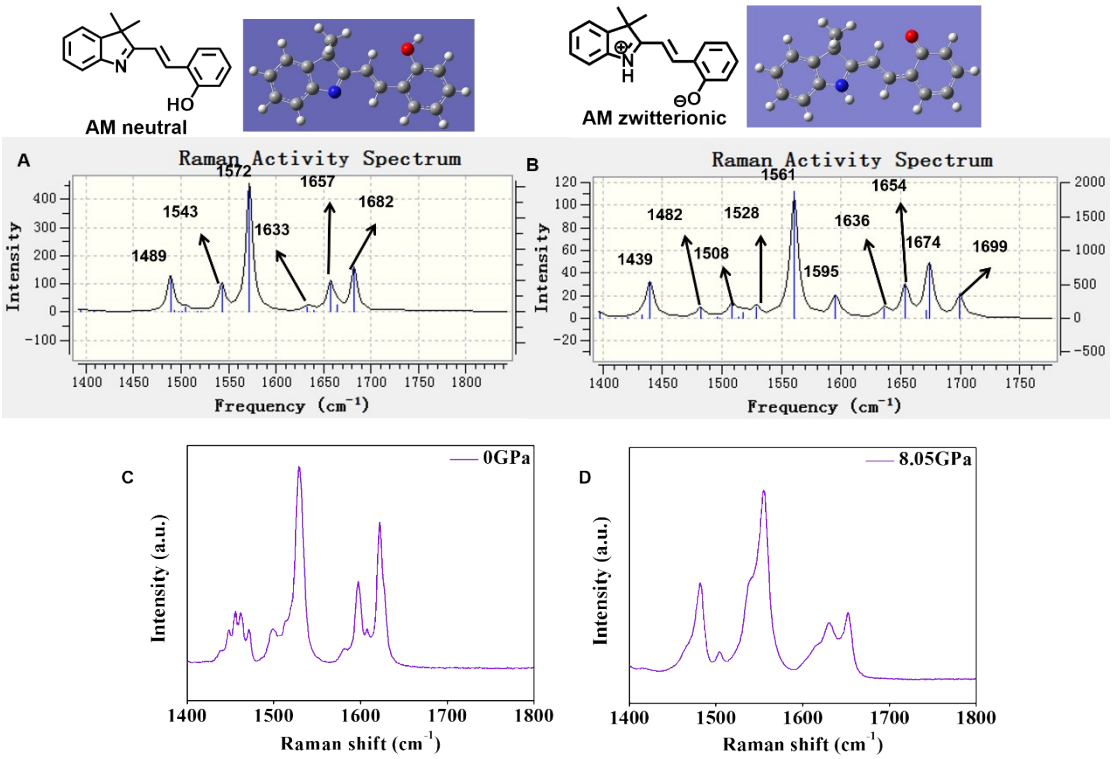

Figure S11. (A) Multi-peaks fitting of the Raman peaks of **AM** in the range of 1500 cm^{-1} to 1600 cm^{-1}. (B, C) The shifting of the fitted peaks of **AM** with pressure. (D) The integrate of fitted Raman spectra of **AM**. (E) The ratio of zwitterionic isomer of **AM** under high pressure (above 6 GPa).

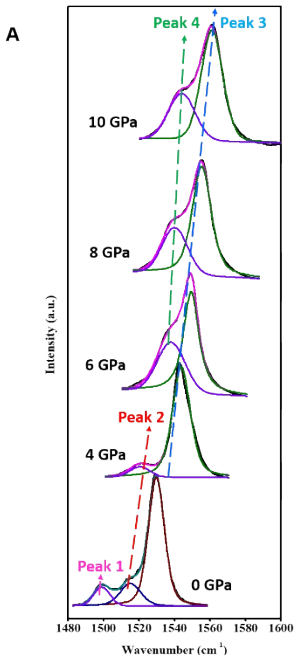

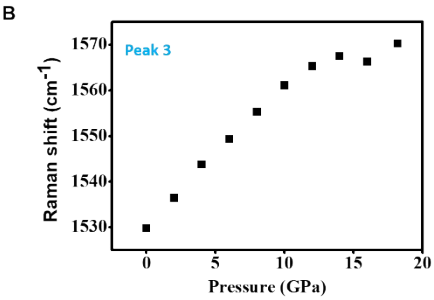

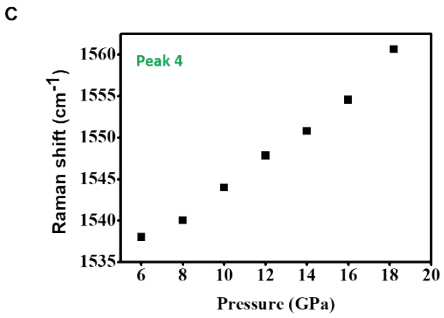

D

Pressure (Gpa)	Area 1 (peak 3)	Area 2 (peak 4)	Ratio (%)
6	2.76078E6	1.74442E6	0.73313
8	2.96312E6	1.3343E6	0.66191
10	1.9927E6	974246	0.68007
12	895746.3	394804.9	0.6571
14	422427.1	270110.9	0.73546
16	304730.8	175363.8	0.71445
18.2	157718	93093.46	0.7196

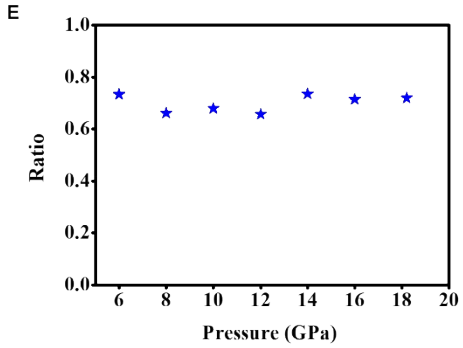

Just like **AM-N**, through comparing the simulated Raman spectra of neutral and zwitterionic **AM** molecules, we know that the peaks at 1572 cm^{-1} and 1561 cm^{-1} are the characteristic Raman peaks of neutral and zwitterionic **AM** molecules, respectively (Figure S10). In addition, they correspond to Peak 3 and Peak 4 in experimental Raman spectra, respectively (Figure S11A-C). Therefore, we will utilize the integrate of Peak 3 and Peak 4 (Figure S11D) to represent the contents of zwitterionic and neutral isomers of **AM**, respectively. Owing to the low Raman activity of zwitterionic isomer of AM (namely the Raman peak intensity is low), the characteristic Raman peak (Peak 4) of zwitterionic isomer of **AM** is obviously observed only when pressure reaches 6 GPa. Thus, we can only estimate the ratio of zwitterionic isomer of **AM** in the pressure region from 6 GPa to 18 GPa. The ratio of zwitterionic **AM** ($\omega_{\text{zwitterionic isomer}}$) under high pressure could be also roughly estimated by following equation:

$$\omega_{\text{zwitterionic isomer}} = \text{Height of Peak 4/(integrate of Peak 3+ integrate of Peak 4)}\times 100\% \ldots 1$$

Equation 1 can be expressed as follow:

$$\omega_{\text{zwitterionic isomer}} = 1/(1+ \text{integrate of Peak 3/ integrate of Peak 4})\times 100\% \ldots 2$$

Similarly, considering the correction factor (*f*) and the Equation 2 can be expressed as follow:

$$\omega_{\text{zwitterionic isomer}} = 1/(1+ \text{Experimental integrate of Peak 3/ Experimental integrate of Peak 4} \times f)\times 100\% \ldots 3$$

Note: The correction factor (*f*) is obtained through the Raman activity of simulated Raman peak for zwitterionic **AM** (Figure S10) divided by the Raman activities of simulated Raman peak (Figure S10) for neutral **AM**.

$$f = (1878)/8178 = 0.23$$

Figure S12. In-situ absorption spectra (A) and Raman spectra (B, C) of the **AM** crystal in the DAC with decreasing pressure.

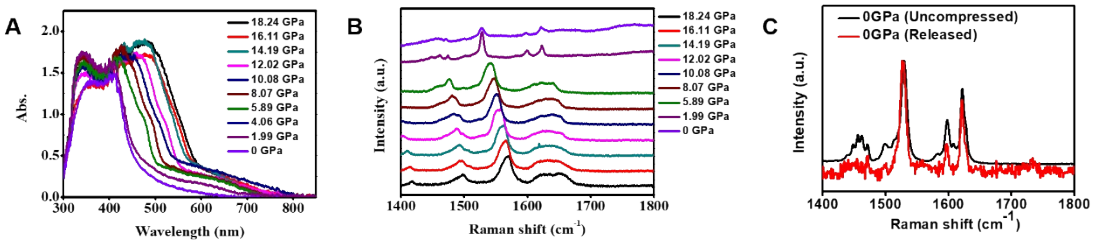

The experimental analysis OM-N under pressure

Figure S13. Simulated (A and B) and experimental (C and D) Raman spectra of **OM-N** in neutral form and zwitterionic isomers. The calculations are based on B3LYP/6-31G (d,p), Gaussian 09 package.[3]

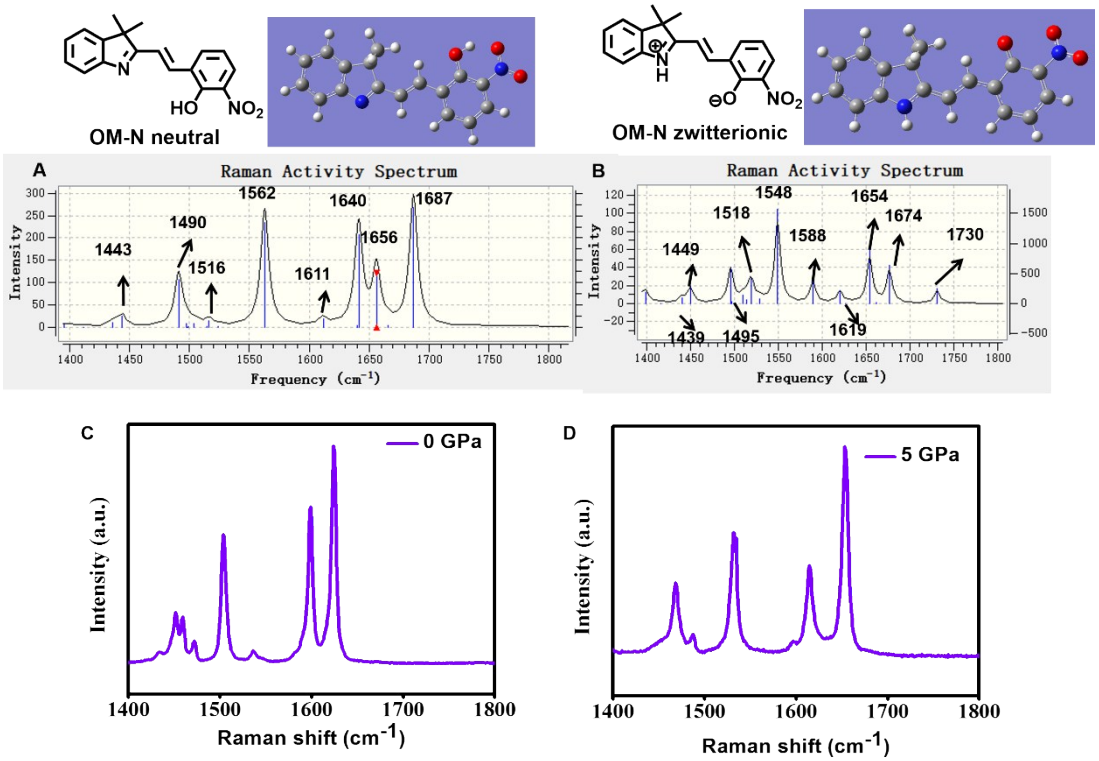

Figure S14. In-situ absorption spectra (A) and Raman spectra (B) of the **OM-N** crystal in the DAC with decreasing pressure.

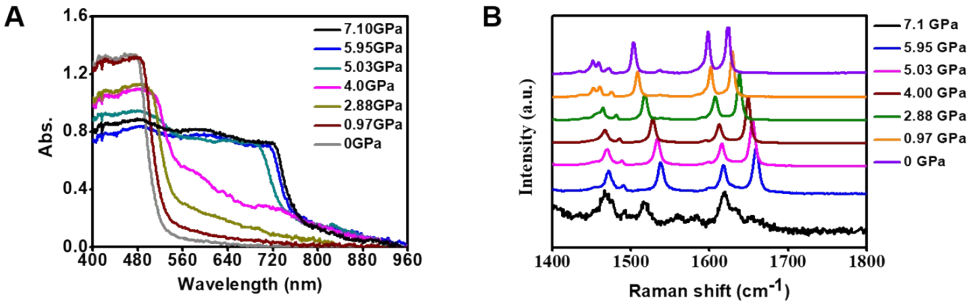

The experimental analysis AM-N-C under pressure

Figure S15. Simulated (A and B) and experimental (C and D) Raman spectra of **AM-N-C**. The calculations are based on B3LYP/6-31G (d,p), Gaussian 09 package. [3]

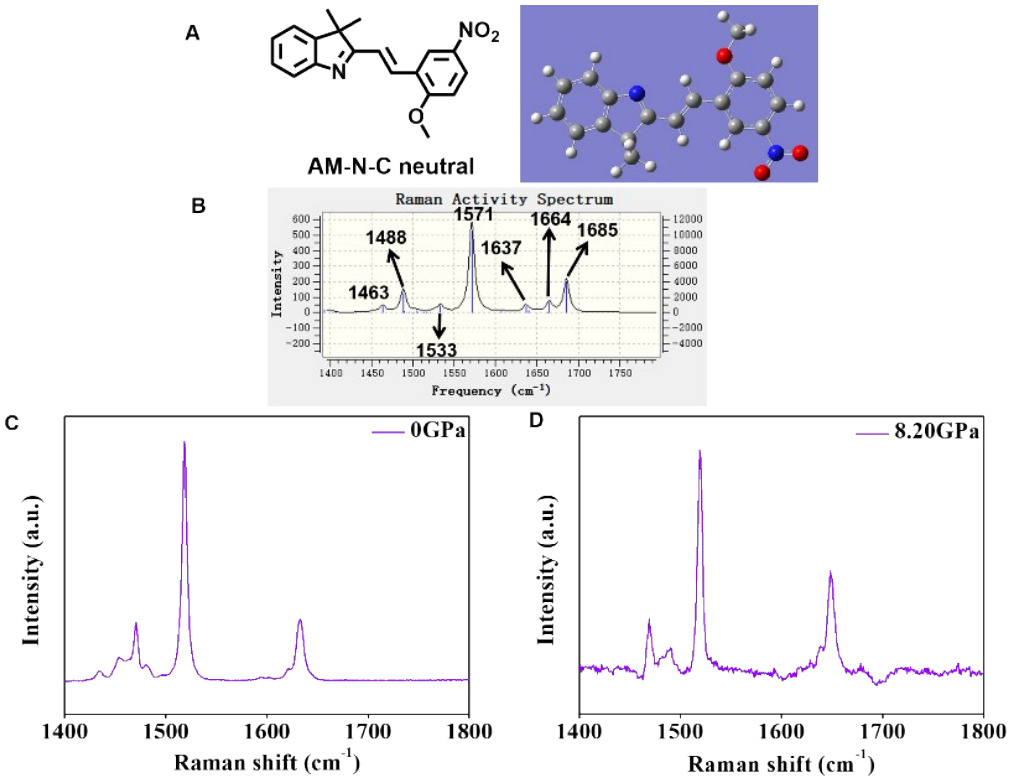

Figure S16. The difference values between the wavelength at absorption starting-point and main absorption turning-point of **AM-N-C** under different pressure

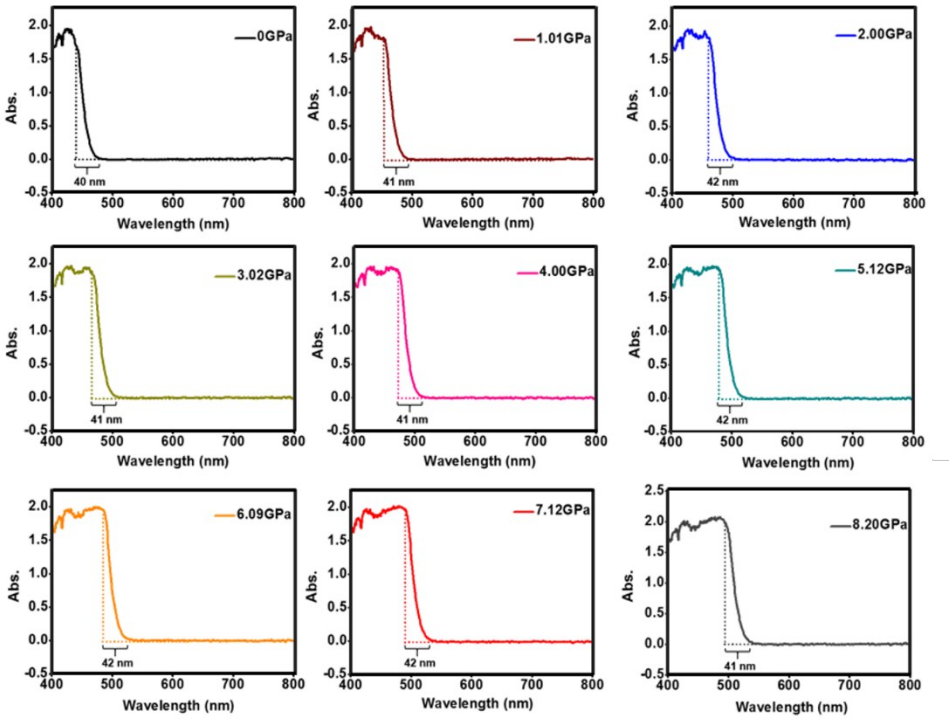

Without chemical transition, pressure should show monotonous or linear effects on molecular conformation and intermolecular distance. As a result, the absorption spectra of **AM-N-C** exhibit monotonously red-shift with pressure without any obvious broadening (Figure S16), further proving the proton transfer process of **AM-N, AM** and **OM-N**.

Figure S17. Shift of the main Raman peaks (A) with increasing pressure and in-situ absorption spectra (B) and Raman spectra (C) of the **AM-N-C** crystal with decreasing pressure.

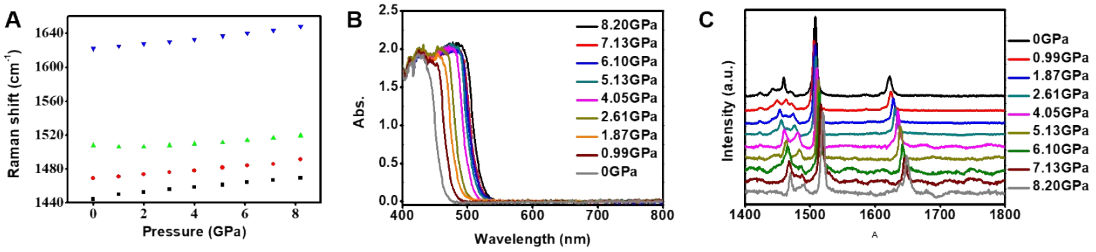

The calculated results of AM-N, AM and OM-N

The below data of the crystals were calculated based on the CASTEP module in Material Studio.[5-6] The generalized gradient approximation (GGA) with Perdew Burke Ernzerhof (PBE) was used to describe the exchange-correlation effects. This calculation was done with plane wave set using Norm-conserving pseudopotentials. For self-consistent field (SCF) calculation, the energy tolerance was set to 1.0 $\times 10^{-6}$ eV per atom.

Figure S18. The Final energy of unit cells for **AM-N** (A, B), **AM** (C, D) and **OM-N** (E, F) with different cut-off energy and K-points.

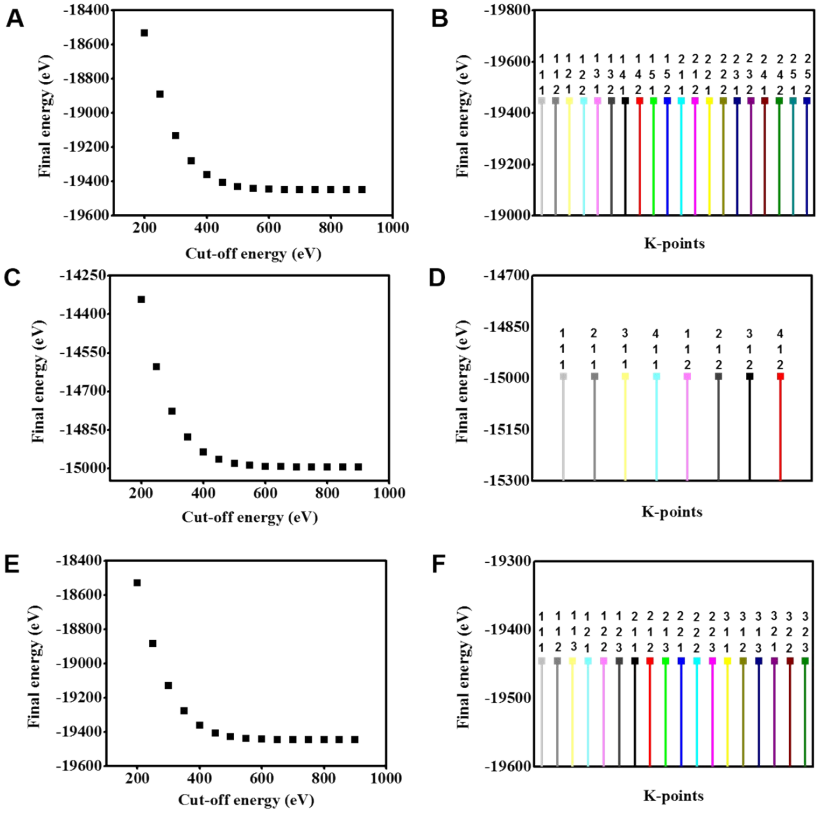

Based on Figure S18, the final energies of unit cells for **AM-N, AM and OM-N** are all stationary when cut-off energy is higher than 600 eV. Moreover, the final energies of unit cells for **AM-N, AM and OM-N** are all stationary no matter the K-points change.

Thus, for geometry optimization, we have used the cut-off energy (750 eV) for all unit

cells as K-points are (1 2 1), (2 1 1) and (1 1 1) for **AM-N, AM and OM-N**, respectively. And the energy tolerance was 1.0 $\times 10^{-5}$ eV per atom with the force tolerance of 0.03 eV/Å, a maximum displacement of 1.0 $\times 10^{-3}$ Å, and a maximum stress tolerance of 0.05 GPa.

Figure S19. View the crystal packing of **AM-N** (A, B, C), **AM** (D, E, F) and **OM-N** (G, H, I) along a-axis (red solid line), b-axis (green solid line) and c-axis (blue solid line) direction.

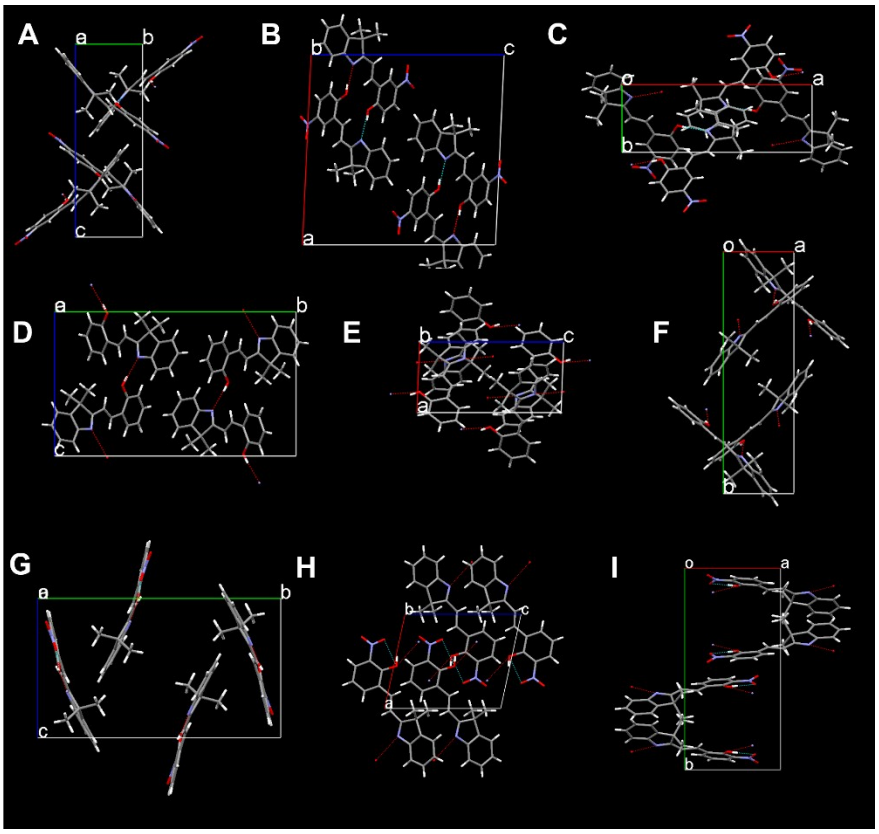

The vectors of intermolecular hydrogen bond can be rewritten in terms of three different components on directions of unit cells. As shown in Figure S19, we find that viewing along a-axis, b-axis and c-axis, intermolecular hydrogen bonds are better parallel to a-axis of all unit cells. The repulsion between hydrogen bond donor and acceptors will make the a-axis less compressible. Thus, the repulsion between hydrogen bond donor and acceptors will make the *a*-axis less compressible.

Table S2. The calculated volume and volume changes upon pressure in the unit cell of AM-N, AM and OM-N (red letters: volume and volume changes at the inflection point, 5 GPa, 30 GPa and 14 GPa for AM-N, AM, OM-N respectively).

AM-N			AM			OM-N		
Pressure (GPa)	Volume (Å^3)	Volume changes(Å^3)	Pressure (GPa)	Volume (Å^3)	Volume changes(Å^3)	Pressure (GPa)	Volume (Å^3)	Volume changes(Å^3)

0	1710.95		0	1621.47		0	1744.1	
1	1573.04	137	5	1179.76	442	2	1439.11	305
2	1453.84	120	10	1046.13	133	4	1312.17	127
3	1367.98	86	15	966.7583	80	6	1231.79	81
4	1318.06	49	20	912.49	54	8	1177.41	54
5	1276.37	42	25	871.271	41	10	1133.14	44
6	1241.38	35	30	836.966	35	12	1086.85	47
7	1217.83	24	35	808.727	28	14	1064.44	22
8	1192.89	25	40	784.183	24	16	1039.16	25
						18	1016.11	23

Table S3. The calculated lattice parameters of the AM-N crystal under different pressure.

Pressure (GPa)	a (Å)	b (Å)	c (Å)	alpha (°)	beta (°)	gamma (°)
0	16.5465	5.983	17.3048	90	92.8917	90
1	16.3289	5.7756	16.6905	90	92.0753	90
2	16.0652	5.5758	16.2342	90	91.2785	90
3	15.9079	5.4323	15.8602	90	89.8106	90
4	15.7887	5.3438	15.623	90	89.3586	90
5	15.7893	5.2862	15.2926	90	89.5584	90
6	15.6619	5.2409	15.1238	90	89.6781	90
7	15.5941	5.2163	14.9723	90	89.3986	90
8	15.4868	5.1842	14.8591	90	89.2553	90

Table S4. The calculated lattice parameters of the AM crystal under different pressure.

Pressure (GPa)	a (Å)	b (Å)	c (Å)	alpha (°)	beta (°)	gamma (°)
0	6.2007	21.3698	12.2383	90	89.095	90
5	5.9955	17.1957	11.4679	90	93.762	90
10	5.9815	15.6332	11.2045	90	93.17006	90
15	6.033	15.1475	10.5847	90	91.8934	90
20	5.9936	14.5883	10.44	90	91.5789	90
25	5.9663	14.1607	10.3158	90	91.4552	90
30	5.9598	13.7966	10.18	90	90.8107	90
35	5.9378	13.5127	10.0801	90	90.6801	90
40	5.9181	13.2706	9.9854	90	90.5654	90

Table S5. The calculated lattice parameters of the OM-N crystal under different pressure.

Pressure	a (Å)	b (Å)	c (Å)	alpha (°)	beta (°)	gamma (°)

(GPa)						
0	8.8956	18.6336	10.8312	90	103.7227	90
2	8.5718	16.4614	10.3995	90	101.2698	90
4	8.4246	15.6652	10.0997	90	100.1151	90
6	8.3174	15.1977	9.8728	90	99.2387	90
8	8.2533	14.7826	9.7659	90	98.8168	90
10	8.1958	14.4573	9.6693	90	98.4925	90
12	8.1454	14.1907	9.5893	90	98.2849	90
14	8.1783	13.7086	9.6494	90	100.2858	90
16	8.1501	13.4791	9.6115	90	100.2091	90
18	8.1199	13.2927	9.5633	90	100.1349	90

The data of Table S3-S5 directly illustrate that the compression of AM-N, AM and OM-N crystal structures is anisotropic.

Figure S20. The simulated N…O distances of the AM-N, AM and OM-N crystals under different pressure.

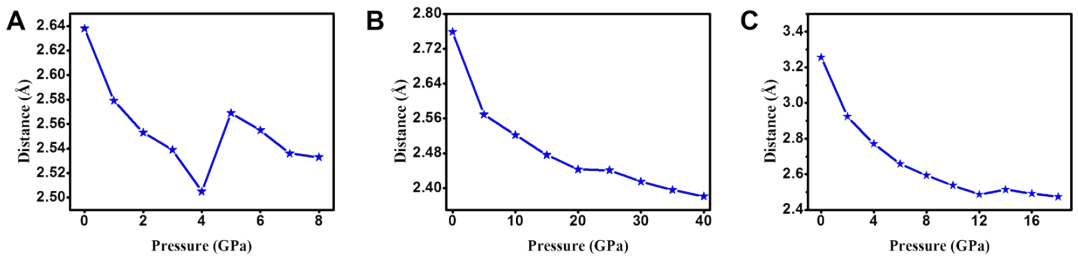

The distance changes of N…O illustrate that under low pressure region (before the inflection point, 5 GPa, 30 GPa and 14 GPa for AM-N, AM, OM-N respectively), N atom and O atom are approaching to each other (Figure S20) with shortening the distance of N…H hydrogen bonds (Figure 6). When pressure reaches the inflection point, the optimized crystal structures of AM-N, AM, OM-N shows that though the proton is bonded to the nitrogen atoms simultaneously and the distance of N…O are increased abruptly, the distance of N…O have been efficiently shortened and the proton is still strongly contacted to the oxygen atom (Figure 6, S20 and S21). Therefore, there should not be a complete proton transfer process of OH…N hydrogen bonds in actual compression of AM-N, AM and OM-N crystals, it should be actually the share of the proton by deviating gradually to the proton acceptor from proton donor.

Figure S21. Optimized crystal structures of **AM-N, AM and OM-N** under different pressure.

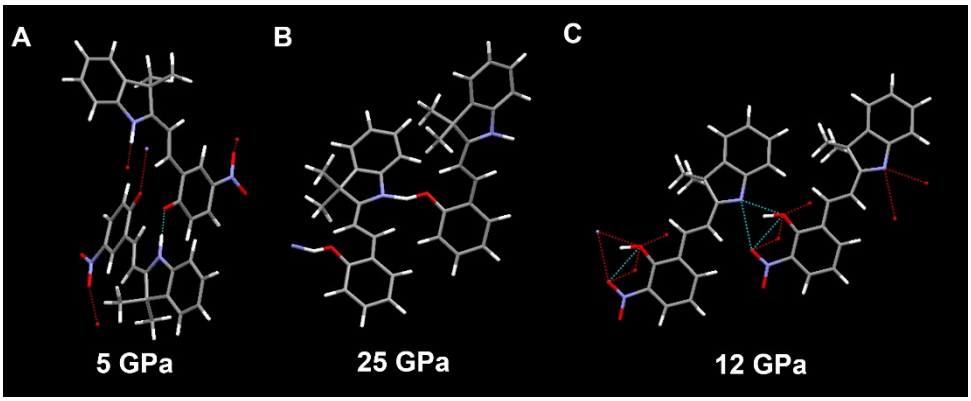

Though pressure reaches 5 GPa for **AM-N** and 14 GPa for **OM-N**, the optimized crystal structure of these two molecules shows that the proton is bonded to nitrogen atoms simultaneously (Figure S25A and S25C), indicating that it might be a full cleavage of hydrogen bond and nitrogen. However, when we analyze it more, it could be found that the distance between proton and still close (Figure 7D-7F). Then, we also observe that in **AM** at 25 GPa, the proton is strongly connected to oxygen and nitrogen atoms (Figure S25B). Therefore, there should not be complete proton transfer process between proton-donor and proton-acceptor in actual compressed condition, it should actually be the share of the proton by deviating gradually to the proton acceptor from proton donor.

References

(1) Roxburgh, C. J.; Sammes, P. G.; Abdullah, A. Dyes Pigm. 2009, 83, 31-50.

(2) Wang, Y.; Li, M.; Zhang, Y. -M.; Yang, J.; Zhu, S.; Sheng, L.; Wang, X.; Yang B.; Zhang, S. X. -A. Chem. Commun. 2013, 49, 6587-6589.

(3) Frisch, M. J.; Trucks, G. W.; Schlegel, H. B.; Scuseria, G. E.; Robb, M. A.; Cheeseman, J. R.; Scalmani, G.; Barone, V.; Mennucci, B.; Petersson, G. A.; Nakatsuji, H.; Caricato, M.; Li, X.; Hratchian, H. P.; Izmaylov, A. F.; Bloino, J.; Zheng, G.; Sonnenberg, J. L.; Hada, M.; Ehara, M.; Toyota, K.; Fukuda, R.; Hasegawa, J.; Ishida, M.; Nakajima, T.; Honda, Y.; Kitao, O.; Nakai, H.; Vreven, T.; Montgomery, J.; Peralta, J. E.; Ogliaro, F.; Bearpark, M.; Heyd, J. J.; Brothers, E.; Kudin, K. N.; Staroverov, V. N.; Kobayashi, R.; Normand, J.; Raghavachari, K.; Rendell, A.; Burant, J. C.; Iyengar, S. S.; Tomasi, J.; Cossi, M.; Rega, N.; Millam, J. M.; Klene, M.; Knox, J. E.; Cross, J. B.; Bakken, V.; Adamo, C.; Jaramillo, J.; Gomperts, R.; Stratmann, R. E.; Yazyev, O.; Austin, A. J.; Cammi, R.; Pomelli, C.; Ochterski, J. W.; Martin, R. L.; Morokuma, K.; Zakrzewski, V. G.; Voth, G. A.; Salvador, P.; Dannenberg, J. J.; Dapprich, S.; Daniels, A. D.; Farkas, O.; Foresman, J. B.; Ortiz, J. V.; Cioslowski, J.; Fox, D. J. Gaussian 09, Revision A. 02; Gaussian, Inc: Wallingford, CT 2009.

(4) Ni, B. -B.; Wang, K.; Yan, Q.; Chen, H.; Ma Y.; Zou, B. Chem. Commun. 2013, 49, 10130-10132.

(5) Materials Studio CASTEP, M. Segall, M. Probert, C. Pickard, P. Hasnip, S. Clark, K. Refson, J.

R. Yates, M. Payne.
(6) "First principles methods using CASTEP"， S. J. Clark, M. D. Segall, C. J. Pickard, P. J. Hasnip, M. J. Probert, K. Refson, M. C. Payne. Zeitschrift fuer Kristallographie, 220(5-6), 2005, 567-570.